molecular pharmaceutics

pubs.acs.org/molecularpharmaceutics

Article

Sortase-Mediated Site-Specific Conjugation and ^{89}Zr-Radiolabeling of Designed Ankyrin Repeat Proteins for PET

Rachael Fay, Imre Törő, Anna-Lena Schinke, Branko Simic, Jonas V. Schaefer, Birgit Dreier, Andreas Plückthun, and Jason P. Holland*

Cite This: *Mol. Pharmaceutics* 2022, 19, 3576−3585

Read Online

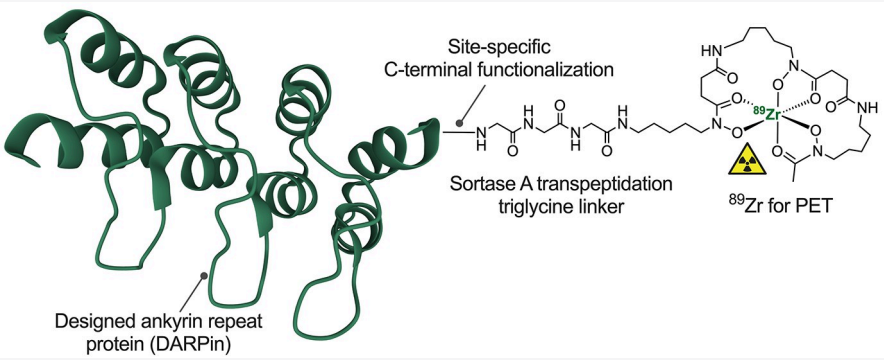

ABSTRACT: Designed ankyrin repeat proteins (DARPins) are genetically engineered proteins that exhibit high specificity and affinity toward specific targets. Here, the G3-DARPin, which binds the HER2/*neu* receptor, was site-specifically modified with enzymatic methods and ^{89}Zr-radiolabeled for applications in positron emission tomography (PET). Sortase A transpeptidation was used to install a desferrioxamine B (DFO) chelate bearing a reactive triglycine group to the C-terminal sortase tag of the G3-DARPin, and ^{89}Zr-radiolabeling produced a novel ^{89}ZrDFO-G3-DARPin radiotracer that can detect HER2/*neu*-positive tumors. The triglycine probe, DFO-Gly$_3$ (**1**), was synthesized in 29% overall yield. After sortase A transpeptidation and purification from the nonfunctionalized protein component, the DFO-G3-DARPin product was radiolabeled to give ^{89}ZrDFO-G3-DARPin. Binding specificity was assessed in HER2/*neu*-expressing BT-474 and SK-OV-3 cellular assays. The pharmacokinetics, tumor uptake, and specificity of ^{89}ZrDFO-G3-DARPin were measured *in vivo* by PET imaging and confirmed by final time point (24 h) biodistribution experiments in female athymic nude mice bearing BT-474 xenografts. Sortase A transpeptidation afforded the site-specific and stoichiometrically precise functionalization of DFO-G3-DARPin with one chelate per protein. The modified DFO-G3-DARPin was purified from the nonfunctionalized DARPin by using Ni-NTA affinity chromatography. ^{89}ZrDFO-G3-DARPin was obtained with a radiochemical purity of >95% measured by radio-size-exclusion chromatography. BT-474 tumor uptake at 24 h postadministration reached 4.41 ± 0.67 %ID/g (n = 3) with an approximate ∼70% reduction in tumor-associated activity in the blocking group (1.26 ± 0.29 %ID/g; 24 h postadministration, n = 5, P-value of <0.001). Overall, the site-specific, enzyme-mediated functionalization and characterization of ^{89}ZrDFO-G3-DARPin in HER2/*neu* positive BT-474 xenografts demonstrate that DARPins are an attractive platform for generating a new class of protein-based radiotracers for PET. The specific uptake and retention of ^{89}ZrDFO-G3-DARPin in tumors and clearance from most background tissues produced PET images with high tumor-to-background contrast.

KEYWORDS: *positron emission tomography, DARPin, ^{89}Zr, HER2/neu, site-specific bioconjugation, sortase*

■ INTRODUCTION

Monoclonal antibodies (mAbs) have been widely used in positron emission tomography (PET) since the 1990s.[1,2] The high specificity and affinity for target binding and their prolonged circulation time in the blood pool mean that mAbs are excellent scaffolds for designing radiotracers. However, the large size of IgG$_1$ immunoglobulins (∼150 kDa) limits tissue penetration and accumulation of mAbs in tumors is slow, often requiring 3 days in rodent models and over a week in humans before peak uptake and contrast is observed.[1,3−10] A simple way to reduce serum clearance time is to use low molecular weight antibody mimics, such as immunoglobulin fragments or genetically engineered proteins like designed ankyrin repeat

Special Issue: Antibody-Based Imaging and Therapy for Precision Medicine

Received: February 19, 2022
Revised: April 5, 2022
Accepted: April 6, 2022
Published: April 18, 2022

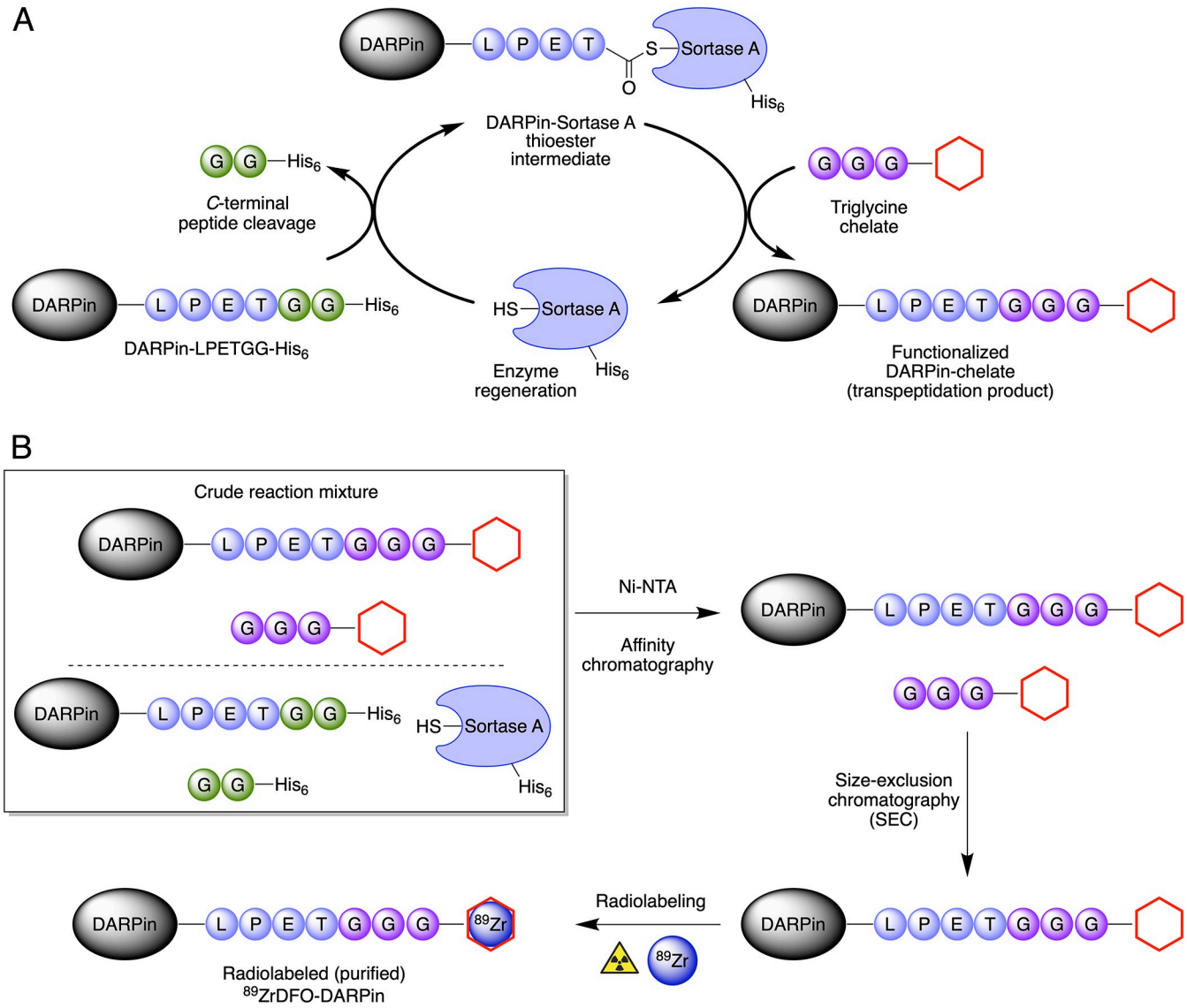

Figure 1. (A) Schematic showing the mechanism of sortase A-mediated transpeptidation of a DARPin-LPETGG-His$_6$ with a chelate (red hexagon) bearing a triglycine group. Note that the reaction is reversible but only the forward process is shown for clarity. (B) Multistep purification that allows isolation of the functionalized DARPin-chelate from reaction byproducts and starting materials.

proteins (DARPins).[11−13] In comparison to radiotracers that use full-length mAbs, the rapid circulation and clearance of small antibody mimics could improve image contrast and provide access to same day PET imaging in the clinic.[14,15]

DARPins are small (11−20 kDa), extremely stable antibody mimics that are synthetic consensus proteins constructed using the ankyrin repeat protein fold.[13,16,17] Ankyrin repeat proteins consist of stacked ankyrin motifs, consisting of a β-turn followed by antiparallel α-helices. The N-terminal and C-terminal capping repeats (caps) shield a more hydrophobic internal core of the protein. The internal repeats carry randomized residues that are selected to specifically interact with the target.[13] DARPins display high stability toward denaturation by either heat or exposure to guanidine hydrochloride and are not prone to aggregation at high concentrations.[17−19] On the basis of their biophysical properties, DARPins have been proposed as a robust platform for further chemical functionalization and radiolabeling.

The DARPin G3 possesses picomolar affinity (91 ± 1 pM) for domain 4 of HER2/*neu*.[20] The amino acids involved in DARPin G3 binding to HER2/*neu* are predominantly aromatic (Tyr, Phe) or lipophilic (Ala, Leu, Ile) residues located in the first and second ankyrin repeats and the C-terminal cap.[21] Previous structure determination indicated that the G3-DARPin binds to an epitope of HER2/*neu* that is adjacent to, but not overlapping with, the binding site of trastuzumab.[21] This feature means that a PET radiotracer based on the G3-DARPin could be used to image the response of HER2/*neu* positive breast cancer patients who are undergoing treatment with trastuzumab.[22,23]

Radiolabeled DARPins have been used in single-photon emission computed tomography (SPECT). In the first report, Zahnd et al. radiolabeled the G3-DARPin and related constructs with $[^{99m}Tc(CO)_3]^+$ via a hexahistidine (His$_6$) tag-specific approach.[20,24] Goldstein et al. used direct radioiodination (^{123}I or ^{125}I) of tyrosine residues on the G3-DARPin and, in the same work, also performed site-specific ^{111}In-

https://doi.org/10.1021/acs.molpharmaceut.2c00136
Mol. Pharmaceutics 2022, 19, 3576−3585

radiolabeling of a DOTA-maleimide chelate located at the C-terminal cysteine.[15,20,25] Vorobyeva et al.[15] reported both ^{125}I and ^{99m}Tc radiolabeling of DARPin9_29, which binds to domain 1 of HER2/*neu*.[21] In 2019, an ^{124}I-radiolabeled G3-DARPin was tested for applications in PET.[26] Direct iodination of Tyr residues that are involved in target binding can negatively impact the immunoreactivity of protein-based radiotracers.[21] Deyev et al. reported ^{68}Ga, ^{111}In, ^{57}Co, and ^{125}I radiolabeling studies using a DARPin that binds to the epithelial cell adhesion molecule (EpCAM).[27] Recently, Bragina et al. also reported exciting data from a phase I trial of ^{99m}Tc-(HE)$_3$-labeled small protein derived from an albumin binding domain for imaging of HER2/*neu* expression in breast cancer confirming the safety and excellent performance of this SPECT probe[28] that also justifies further development of DARPin-based radiotracers.

Sortase A transpeptidation enables triglycine probes to be conjugated to the protein of interest via the formation of a new peptide bond.[29] The five amino acid motif, LPXTG (where X is typically glutamic acid (E) but can vary), is required for recognition of the protein substrate by the active site of the sortase A enzyme. Sortase A-mediated conjugation reactions can be performed at either the N- or C-terminus of a protein substrate.[30,31] To employ sortase A in the synthesis of radiolabeled G3-DARPins, either the LPXTG recognition motif must be installed at the C-terminus or a polyglycine group at N-terminus of the protein.[29−31] In this work, we elected to use C-terminus functionalization because clones of the DARPin-LPETGG-His$_6$ construct were available.[18] A mechanistic scheme of the sortase A transpeptidation of DARPin-LPETGG-His$_6$ construct bearing a C-terminal LPETG motif and a conjoined His$_6$ tag is shown in Figure 1A. In the first step of the reaction, a sulfhydryl group in the active site of sortase A acts as a nucleophile to cleave the threonine−glycine (Thr-Gly) peptide bond,[32] resulting in a reactive thioester intermediate of this Thr, which can undergo nucleophilic attack by a compound bearing a triglycine group to produce the transpeptidation product and the regenerated enzyme.[32] Notably, in our reaction design both the sortase A enzyme and the nonfunctionalized G3-DARPin contain His$_6$ tags. During the enzymatic transpeptidation, the His$_6$ tag of the G3-DARPin is cleaved, and the functionalized DARPin can therefore be separated from the nonfunctionalized G3 DARPin using Ni-NTA affinity chromatography (Figure 1B).[33] Similar purification strategies involving sortase A-mediated transpeptidations have been used to prepare ^{64}Cu, ^{111}In, and ^{68}Ga conjugates of camelid single-domain antibody fragments (sdAbs) and single-chain variable fragments (scFv).[34,35]

In this work, our goal was to evaluate the potential of radiolabeled DARPins as a platform for building diagnostic PET radiotracers. We report the site-specific functionalization of G3-DARPin with a triglycine probe based on desferrioxamine B (DFO) that can complex different radionuclides including ^{68}Ga^{3+} and ^{89}Zr^{4+} for PET.

■ MATERIALS AND METHODS

Full experimental details and characterization data are presented in the Supporting Information.

Chelate Synthesis. Triglycine functionalized DFO-Gly$_3$ (compound **1**) was synthesized as described in the experimental section (Supplemental Scheme 1 and Supplemental Figures 1−4). Compounds were fully characterized with ^{1}H and ^{13}C{^{1}H} NMR spectroscopy, mass spectrometry, and analytical high-performance liquid chromatography (HPLC).

Radiochemistry. [^{89}Zr][Zr(C$_2$O$_4$)$_4$]$^{4-}$(aq) was obtained as a solution in ∼1.0 M oxalic acid from PerkinElmer (Boston, MA, manufactured in The Netherlands) and was used without further purification. [^{68}Ga][Ga(H$_2$O)$_6$]Cl$_3$(aq) was obtained from ^{68}Ge/^{68}Ga-generators (Eckert & Ziegler, model IGG100 gallium-68 generator) and eluted with 0.1 M HCl(aq). The eluted ^{68}Ga activity was trapped and purified by using a strong cation exchange column (Strata-XC, [SCX], Eckert & Ziegler). [^{68}Ga][Ga(H$_2$O)$_6$]Cl$_3$(aq) was eluted from the SCX cartridge by using a solution containing 0.13 M HCl(aq) and ∼5 M NaCl(aq) (SCX eluent).

Protein Expression and Purification. Proteins were expressed in *E. coli* and purified by using immobilized metal ion affinity chromatography as described previously (see supplementary methods).[36]

Western Blot Monitoring of Enzyme-Mediated Reactions. The G3-DARPin-LPETGG-His$_6$ bearing a sortase tag (0.52 nmol, 40 μM) was incubated with varying concentrations of sortase A (4−120 μM) and a Gly$_3$ probe (200−4000 μM) in 50 mM Tris-HCl, 150 mM NaCl, CaCl$_2$ (10 mM) at pH 7.9. Reactions were mixed and centrifuged (4300 rpm, 30 s) before incubation overnight at 37 °C with shaking (400 rpm). Reactions were analyzed by SDS−PAGE and anti-His$_6$ Western blot (see Supporting Information for antibodies details).

Protein Functionalization. G3-DARPin-LPETGG-His$_6$ (38 nmol) was incubated with sortase A (38 nmol, 1 equiv) and the triglycine probe (1.9 μmol, 50 equiv) in 50 mM Tris-HCl, 150 mM NaCl, 10 mM CaCl$_2$ at pH 7.9. After incubation overnight at 37 °C with shaking (400 rpm), the reaction was purified with reverse Ni-NTA affinity chromatography and SEC.

Stability Studies. The stability of ^{89}ZrDFO-G3-DARPin with respect to change in radiochemical purity (RCP) was investigated by incubation in an excess of diethylenetriamine pentaacetate (DTPA, pH 7.4, 14 mM, 150- to 180-fold excess), in human serum at 37 °C, and in the formulation buffer (PBS + 0.1% BSA, pH 7.4).

Cellular Binding Studies. For cell binding assays, two HER2/*neu* expressing cell lines were used: the human ductal carcinoma cell line BT-474 (American Type Culture Collection [ATCC-HTB-20], Manassas, VA) and the human ovarian adenocarcinoma cell line SK-OV-3 (American Type Culture Collection [ATCC-HTB-77], Manassas, VA). Immunoreactivity was determined using a procedure adapted from Lindmo et al.[37]

Animals and Xenograft Models. Animal experiments were conducted in accordance with an experimentation license approved by the Zurich Canton Veterinary Office, Switzerland. Female athymic nude mice (Crl:NU(NCr)-*Foxn1^{nu}*, 20−25 g, 4−8 weeks old) were obtained from Charles River Laboratories Inc. (Freiburg im Breisgau, Germany). BT-474 tumors were induced on the right shoulder or flank by subcutaneous (sc) injection of approximately 1 × 10^7 cells suspended in 150 μL of a 1:1 v/v mixture of cell media (DMEM/F-12 + penicillin/streptomycin [P/S] + fetal bovine serum [FBS]) and reconstituted basement membrane (Corning Matrigel Basement Membrane Matrix from VWR International). Tumors were monitored over 4.5 weeks and grew to a volume of 25.61 ± 14.40 mm^3 (n = 8).

https://doi.org/10.1021/acs.molpharmaceut.2c00136
Mol. Pharmaceutics 2022, 19, 3576−3585

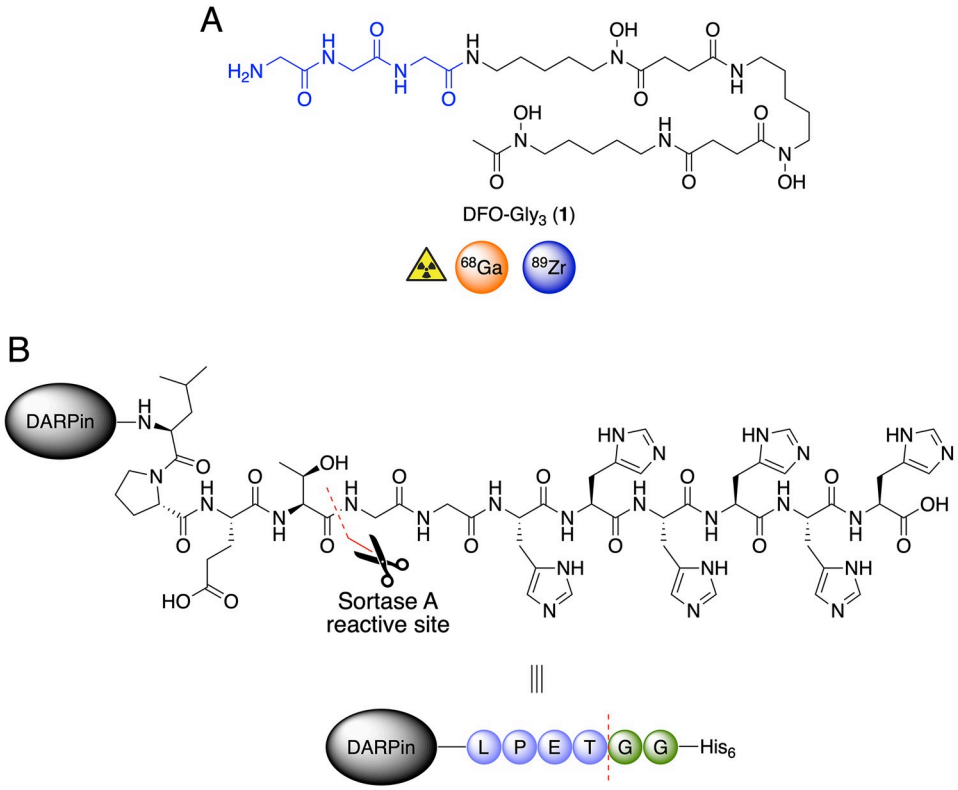

Figure 2. (A) Chemical structure of DFO-Gly$_3$ (**1**). (B) Schematic representation of G3-DARPin-LPETGG-His$_6$ showing the reactive site for sortase A transpeptidation.

Small-Animal PET Imaging. Tumor-bearing mice were randomized before the study. PET imaging experiments were conducted on a Genesis G4 PET scanner (Sofie Biosciences, Culver City, CA) in mice bearing BT-474 xenografts. Doses of ^{89}ZrDFO-G3-DARPin were administered (150 μL, 5−7 μg, 0.34−0.48 nmol, 0.881 ± 0.002 MBq, n = 3, molar activity A_m = 1.84−2.59 MBq nmol^{-1}) via intravenous tail-vein injection. A competitive blocking study was performed with a lower molar activity ^{89}ZrDFO-G3-DARPin produced by supplementing the normal formulation with nonlabeled G3-DARPin_L-PETG (blocking group, 150 μL,1 mg, 70 nmol, 0.876 ± 0.044 MBq, n = 5, A_m = 0.013 MBq nmol^{-1}). Approximately 5 min prior to recording PET images, mice were anesthetized by inhalation of 2−3% isoflurane (Baxter Healthcare, Deerfield, IL)/oxygen gas mixture (∼5 L/min) and placed on the scanner bed. PET images were recorded at various time points between 0 and 24 h postinjection.

Biodistribution Studies. Animals (n = 3−5, per group) were euthanized by exsanguination under anesthesia. Tissue samples were removed, rinsed in water, dried in air for ∼2 min, weighed, and counted on a γ-counter for accumulation of ^{89}Zr-radioactivity.

Statistical Analysis. Data were analyzed by using the unpaired, two-tailed Student's t-test. Differences at the 95% confidence level (P < 0.05) were statistically significant. Statistical analyses were performed with Prism 9 (GraphPad Software LLC, San Diego, CA, USA).

■ RESULTS

Chemical Synthesis. We note that different variations of DFO-glycine probes have recently been reported by the groups of Ploegh[38] and Donnelly.[39] Our triglycine chelate DFO-Gly$_3$ (**1**) is structurally different from these previously reported chelates and was synthesized and isolated in 29% overall yield by using standard chemical transformations. The chemical structure of DFO-Gly$_3$ (**1**) and a schematic representation of G3-DARPin-LPETGG-His$_6$ are shown in Figure 2.

^{68}Ga- and ^{89}Zr-Radiolabeling of Triglycine Probes. Chromatography was used to confirm that compound **1** retained affinity toward ^{68}Ga^{3+} and ^{89}Zr^{4+} metal ions. The radioactive complexes ^{68}Ga-**1**, and ^{89}Zr-**1**$^{+}$ were prepared by using standard radiolabeling reactions and characterized by radioactive high performance liquid chromatography (radioHPLC, Supplemental Figure 5). Product identity was confirmed by comparison of the HPLC retention times versus authenticated, nonradioactive standard complexes.

Sortase A Conjugation Chemistry with G3-DARPin-LPETGG-His$_6$. Next, we analyzed the conditions required to perform sortase A transpeptidation with G3-DARPin-LPETGG-His$_6$. Reactions were followed by using anti-His$_6$-tag Western blots (Figure 3A, Table 1, and Supplemental Figures 6 and 7 for details on the initial DARPin purification). In the Western blot analysis, lanes 1 and 2 correspond to controls with only the sortase A enzyme or the non-functionalized G3-DARPin-LPETGG-His$_6$, respectively (Figure 3A). Lanes 3−5 depict the effect of increasing sortase A equivalents that improved conversion to the triglycine conjugated DARPin as shown by the absence of the G3-DARPin-LPETGG-His$_6$ band. Note that due to a difference in mass, the G3-DARPin-LPETGG-His$_6$ reactant and the triglycine-functionalized product show different migration on gel electrophoresis (SDS−PAGE analysis with Coomassie staining of protein bands: Figure 3B). Increasing the number of equivalents of the triglycine probe also increased the

https://doi.org/10.1021/acs.molpharmaceut.2c00136
Mol. Pharmaceutics 2022, 19, 3576−3585

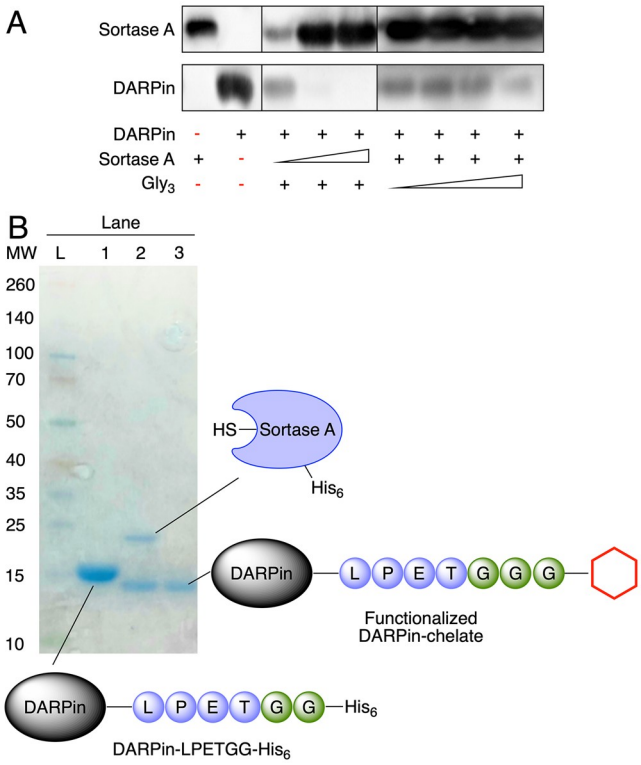

Figure 3. (A) Anti-His tag Western blots showing the sortase A functionalization of the G3-DARPin-LPETGG-His_6 substrate under varying concentrations of enzyme and triglycine substrate. (B) SDS–PAGE analysis with Coomassie staining, following the purification of the DARPin conjugate: lane L = molecular weight ladder; lane 1 = G3-DARPin-LPETGG-His_6; lane 2 = crude rection mixture showing sortase A; lane 3 = purified mixture showing triglycine-functionalized G3-DARPin.

Table 1. Stoichiometric Conditions of Reactants for Sortase A Transpeptidation with the G3-DARPin-LPETGG-His_6 Analyzed by Anti-His_6 Western Blot[a]

	lane								
	1	2	3	4	5	6	7	8	9
	Stoichiometric Equivalents								
DARPin	0	1	1	1	1	1	1	1	1
sortase A	1	0	0.1	1	3	1	1	1	1
Gly_3 probe	0	0	50	50	50	5	10	25	50

[a]See also Figure 3A.

efficiency of the reaction (Figure 3A, lanes 6–9). On the basis of these data, a DARPin:sortase A:triglycine ratio of 1:1:50 was selected for scaling up the bioconjugation reaction between DFO-Gly_3 and G3-DARPin-LPETGG-His_6 to produce sufficient DFO-G3-DARPin for the subsequent radiolabeling and imaging studies (see Supporting Information). We note that the efficiency and kinetics of sortase A mediated bioconjugation reactions are known to be highly dependent on the nature of the substrates and that the robustness of the sortase A enzyme is also a potential limitation in achieving efficient catalytic turnover.[40,41] Quantitative bioconjugation occurs but the total recovered yield of functionalized DARPin depends heavily on the amount of protein loaded onto the purification columns and the extent of nonspecific binding between the protein and the solid-phase extraction cartridges.

^{89}Zr-Radiolabeling of DFO-G3-DARPin. ^{89}ZrDFO-G3-DARPin was produced by ^{89}Zr-radiolabeling DFO-G3-DARPin under standard conditions (see Supporting Information). Initial activities for labeling DFO-G3-DARPin used ~15.8 MBq of a neutralized $[^{89}Zr][Zr(C_2O_4)_4]^{4-}$ (^{89}Zr-oxalate) stock solution. Aliquots of the crude radiolabeling mixture were retained for analysis, and the ^{89}ZrDFO-G3-DARPin was purified by centrifugal spin-filtration. Samples were analyzed by radioTLC (Figure 4A), manual size-exclusion chromatography (SEC) with NAP-10 columns (Figure 4B), and automated radioSEC (Figure 4C). RadioTLC analysis confirmed that ^{89}ZrDFO-G3-DARPin remained at the baseline when using silica gel strips and a diethylenetriamine pentaacetic acid (DTPA) eluent. RadioTLC chromatograms of the crude (Figure 4A, blue trace) and purified (black trace) ^{89}ZrDFO-G3-DARPin product are shown as well as the ^{89}Zr-DFO-Gly_3 probe (purple trace) and $[^{89}Zr(DTPA)]^-$ (red trace) as a control. These radioTLC data indicated near quantitative (>95%) labeling in the crude sample to give ^{89}ZrDFO-G3-DARPin. Manual NAP-10 SEC analysis showed that the purified ^{89}ZrDFO-G3-DARPin radiotracer (Figure 4B, black trace) could be separated from the remaining ^{89}ZrDFO-Gly_3 ($[^{89}Zr]$Zr-**1**$^+$) or "free" $^{89}Zr^{4+}$ impurities (purple trace). Finally, radioSEC analysis confirmed that the purified ^{89}ZrDFO-G3-DARPin was isolated in >95% radiochemical purity (RCP) (Figure 4C). Interestingly, the elution peak for ^{89}ZrDFO-G3-DARPin was at 16.58 mL which differs from that of the unmodified G_3-DARPin-LPETGG-His_6 (15.70 mL). This retention time difference is due to a slight reduction in MW and the serial arrangement of the optical and radioactive detectors. The DFO-Gly_3 conjugation reaction involves the cleavage of an eight amino acid peptide sequence

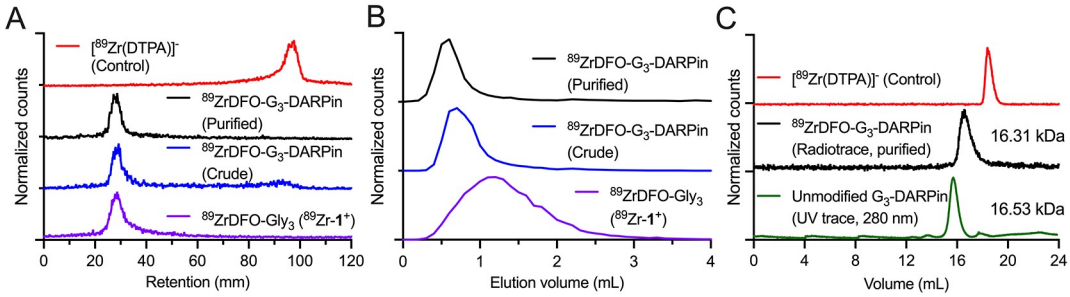

Figure 4. Chromatographic data for ^{89}ZrDFO-G3-DARPin analyzed by (A) radioTLC, (B) radio-NAP-10 SEC, and (C) radioSEC. Purple traces correspond to ^{89}ZrDFO-Gly_3 (^{89}Zr-**1**$^+$), and blue traces and black traces correspond to the crude and purified ^{89}ZrDFO-G3-DARPin, respectively. Red traces show the $[^{89}Zr(DTPA)]^-$ control. In panel C, the green trace shows the UV chromatogram of unmodified G3-DARPin-LPETGG-His_6.

https://doi.org/10.1021/acs.molpharmaceut.2c00136
Mol. Pharmaceutics 2022, 19, 3576–3585

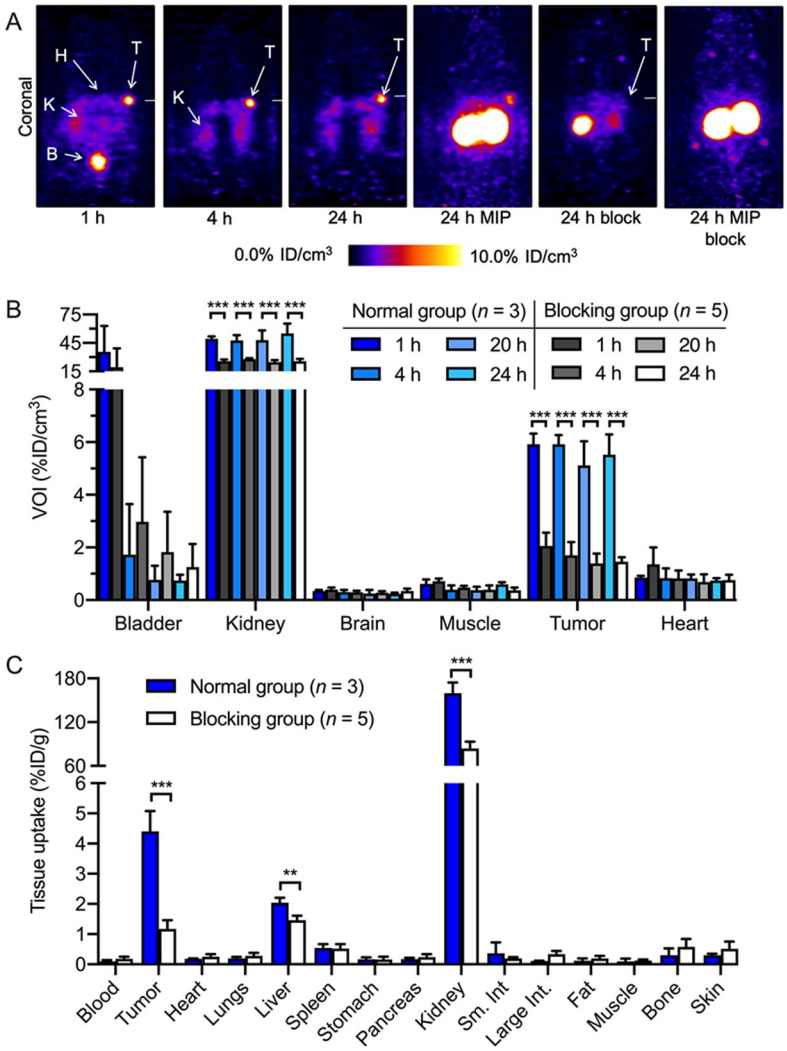

Figure 5. (A) Representative coronal PET images recorded with ^{89}ZrDFO-G3-DARPin in mice bearing BT-474 xenografts.: B = bladder, K = kidney, H = heart, T = tumor, MIP = maximum intensity projection. (B) Quantitative volume-of-interest (VOI) analysis of the PET images. (C) Biodistribution data showing the accumulation of ^{89}ZrDFO-G3-DARPin in different tissues at 24 h.

(GGHHHHHH, MW = 955 Da, 6.5% of DARPin MW) and the addition of DFO-Gly$_3$ for a total decrease in MW of ∼224 g mol^{-1}. This difference in mass (and potentially charge) was also sufficient to resolve DFO-G3-DARPin from the unmodified G3-DARPin-LPETGG-His$_6$ on the SDS−PAGE gel (Figure 3B).

Equivalent radiochemical and chromatographic experiments were performed using ^{68}Ga to produce ^{68}GaDFO-G3-DARPin (Supplemental Figure 8). Labeling with ^{68}Ga demonstrated the flexibility of the chemistry, but we note that the molar activity of these ^{68}Ga-DARPin constructs was too low for imaging purposes. This was primarily due to the use of ^{68}Ga from an old, ex-clinical generator that produced low activity levels. Therefore, in the subsequent *in vitro* and *in vivo* studies we used ^{89}ZrDFO-G3-DARPin.

Stability Studies. ^{89}ZrDFO-G3-DARPin was incubated with excess DTPA, and the stability with respect to change in RCP was monitored by radioTLC (Supplemental Figures 9 and 10). Transchelation of ^{89}Zr to DTPA results in a peak at the solvent front. Under these conditions, ^{89}ZrDFO-G3-DARPin released the activity to the competing DTPA ligand with a half-life of 84.6 ± 9.1 min (Supplemental Figure 10A). Transchelation of $^{89}Zr^{4+}$ ions from DFO is a known phenomenon, and several groups are working toward the synthesis of more stable chelates, but this observation is not usually detrimental to radiotracer performance *in vivo*.[42] Next, we assessed the stability of ^{89}ZrDFO-G3-DARPin in human serum by using radioSEC (Supplemental Figure 10B). In human serum, ^{89}ZrDFO-G3-DARPin was stable over the first 4 h. By the 20 h time point, <25% of the activity was released as a small-molecule ^{89}Zr species but no activity bound to human serum proteins. Radiolabeled DARPins do not circulate in the blood pool after 1 h,[25,43−45] and therefore, the observed serum stability of the ^{89}ZrDFO-G3-DARPin was deemed sufficient for *in vivo* imaging. Finally, ^{89}ZrDFO-G3-DARPin stability in formulation buffer (in PBS + 0.1% bovine serum albumin [BSA]) was analyzed after incubation for 24 h (Supplemental Figure 10C). In total 81% of the ^{89}Zr activity was present in solution as ^{89}ZrDFO-G3-DARPin with no transchelation to BSA observed. Collectively, the stability studies indicated that ^{89}ZrDFO-G3-DARPin displays sufficient stability in human serum or formulation buffer to allow *in vivo* experiments.

Cellular Binding Studies. The biological specificity and immunoreactivity of ^{89}ZrDFO-G3-DARPin toward HER2/*neu*

https://doi.org/10.1021/acs.molpharmaceut.2c00136
Mol. Pharmaceutics 2022, 19, 3576−3585

were assessed by a Lindmo-type cellular saturation binding assay in which a constant amount of ^{89}ZrDFO-G3-DARPin is titrated with increasing number of cells (SKOV-3 or BT-474 cells) until the receptor is in excess and the binding agent is saturated (Supplemental Figures 11 and 12, respectively). Data were consistent across these two cells lines whereby the measured immunoreactive fraction of ^{89}ZrDFO-G3-DARPin was 64.8 ± 7.8% in SK-OV-3 and 63.5 ± 5.9% in BT-474 cells. These values indicate that ^{89}ZrDFO-G3-DARPin retained biological activity and specificity toward the HER2/*neu* receptor.

Small-Animal PET and Biodistribution Studies. Representative planar and maximum intensity project (MIP) coronal PET images recorded after administration of ^{89}ZrDFO-G3-DARPin in mice bearing BT-474 tumors on the right flank are presented in Figure 5A. Additional image data are presented in Supplemental Figures 13−15. A bar chart showing the quantitative volume-of-interest (VOI) analysis of the PET image data is presented in Figure 5B. Uptake of ^{89}ZrDFO-G3-DARPin in BT-474 tumors was easily visualized in the normal group from 1 h postadministration (tumor-VOI = 5.92 ± 0.41 %ID/cm^3, n = 3). In this group of animals, tumor-associated activity remained constant until the end-point image at 24 h (tumor-VOI = 5.52 ± 0.77 %ID/cm^3, n = 3). In the blocking group at 1 h postadministration, as expected, lower tumor accumulation of ^{89}ZrDFO-G3-DARPin was observed (tumor-VOI = 2.06 ± 0.50 %ID/cm^3, n = 5, P < 0.001), and in this group, tumor-associated activity reduced over time to 1.46 ± 0.17 %ID/cm^3 (n = 5, P < 0.05) at 24 h. In both groups, no discernible activity was seen in the heart, even at 1 h p.a. which indicated that ^{89}ZrDFO-G3-DARPin cleared rapidly from circulation. In comparison to the normal group, kidney uptake was reduced in the blocking group (kidney-VOI(1h_normal) = 49.34 ± 2.59 %ID/cm^3, n = 3 versus kidney-VOI(1h_block) = 25.66 ± 1.82 %ID/cm^3, n = 5; P < 0.001).

After the final PET image at 24 h, biodistribution studies were performed (Figure 5C, Supplemental Figure 16, and Supplemental Tables 1 and 2). In the normal group of animals, ^{89}ZrDFO-G3-DARPin radiotracer accumulation in BT-474 tumors was 4.41 ± 0.67 %ID/g (n = 3). In the blocking group the tumor-associated uptake of ^{89}ZrDFO-G3-DARPin decreased by ∼70% to 1.26 ± 0.29 %ID/g (n = 5, P < 0.001). These blocking studies confirmed that ^{89}ZrDFO-G3-DARPin binds specifically to HER2/*neu in vivo*. The difference in kidney accumulation between the two groups was also found to be statistically significant reaching 159.65 ± 14.75 %ID/g (n = 3) in the normal group compared with 82.77 ± 9.44 %ID/g (n = 5, P < 0.001) in the blocking group. These results are consistent with the measured effective half-lives of ^{89}ZrDFO-G3-DARPin in the two groups of animals. The effective half-life in the normal group was 1.26 ± 0.84 h, whereas the blocking dose was more rapidly excreted via the renal system with a measured effective half-life of 0.32 ± 0.12 h (Supplemental Figure 17).

■ DISCUSSION

The rapid tumor accumulation and clearance profile is a potential advantage of using radiolabeled DARPins versus full-length IgG$_1$ monoclonal antibodies as PET radiotracers. Unlike radiolabeled mAbs such as ^{89}Zr-trastuzumab which require prolonged circulation and delayed accumulation,[46,47] ^{89}ZrDFO-G3-DARPin in HER2/*neu*-expressing tumors was visible at 1 h postadministration. Rapid tumor-targeting and clearance from background tissues means that ^{89}ZrDFO-G3-DARPin can potentially give high contrast images and be used for same day PET of patients. Reducing the waiting time between radiotracer administration and PET imaging would also decrease the radiation burden, streamline patient management, and facilitate sequential imaging studies. Other small protein binders such as immunoglobulin fragments[11] or affibodies[48] exist, and the DARPin platform shares many of the positive features with these other classes of compounds such as high affinity and target specificity, rapid clearance, facile bioconjugation, and radiolabeling. Rapid selection of DARPins from ribosome display can facilitate high-throughput radiotracer screening against novel cancer biomarkers.[49] The results obtained using site-specifically labeled ^{89}ZrDFO-G3-DARPin suggest that other radiolabeled DARPins can potentially be developed for applications in imaging and radiotherapy.

Before clinical translation of higher energy emitting DARPin-based PET probes is considered, accumulation in the kidneys requires further investigation. The kidney is the excretory organ for small proteins. Competitive binding experiments indicate that kidney accumulation of ^{89}ZrDFO-G3-DARPin is dependent on the administered (protein) dose. Altai et al.[45] suggested that the high renal accumulation of small binding proteins labeled with [^{99m}Tc]Tc(CO)$_3$, which is a residualizing label that cannot be transported out of the cell again, is associated with an ATP-driven mechanism that may be related to the redistribution of megalin. Megalin is involved in general protein uptake in the kidney and thus independent of the structure of the small binding protein or that of its target. Kidney accumulation in mice could be reduced by administration of rather high concentrations of fructose or maleate prior to radiotracer administration, possibly disturbing energy metabolism in kidney cells.[45] Interestingly, no other compounds were effective. Further studies are required to investigate the mechanism of the nonspecific uptake of radiolabeled DARPins in the kidney and to establish inhibitory mechanisms that can be translated to the clinic.

Sortase A transpeptidation is an attractive method for site-specific functionalizing proteins. Unlike standard conjugation methods that are commonly used to functionalize mAbs, the sortase A chemistry combined with His$_6$-tag separation and size-exclusion chromatography provides a rapid way of separating the functionalized DFO-G3-DARPin product from the unmodified G3-DARPin-LPETGG-His$_6$ starting material. With standard cloning and expression platforms, it is conceptually possible to incorporate the appropriate LPXTG tags into different protein-based scaffolds to leverage sortase A chemistry to make other classes of functionalized proteins for imaging and radiotherapy applications.[30,31] However, a major limitation of employing sortase A conjugation chemistry is the requirement to use high stoichiometric quantities of the enzyme for efficient protein functionalization. This is primarily because the active site of sortase A is not ideally suited to the substrates used. Other limitations include the rather slow conjugation rates observed for the current sortase A-mediated coupling of DFO-Gly$_3$ to our DARPin. This is a potential problem when the goal is to create functionalized proteins that exhibit lower stability, but it underlines the advantage of DARPins in this application. In future studies, these limitations can be overcome by optimizing the sortase A specificity for our

https://doi.org/10.1021/acs.molpharmaceut.2c00136
Mol. Pharmaceutics 2022, 19, 3576−3585

DARPin-LPETGG-His$_6$ and triglycine-chelate substrates. Increasing the reaction rates would also facilitate the functionalization of a wider variety of protein substrates that may be less stable than DARPins.

■ CONCLUSION

Sortase A transpeptidation was used in the site-specific functionalization and ^{89}Zr-radiolabeling of DARPins. The functionalized DFO-G3-DARPin was purified from reaction byproducts and from the unmodified G3-DARPin-LPETGG-His$_6$ by using a combination of affinity chromatography and size-exclusion methods. PET imaging and biodistribution studies using ^{89}ZrDFO-G3-DARPin in BT-474 tumor-bearing mice showed high specificity for the HER2/*neu*-target with excellent tumor-to-background tissue contrast. Kidney uptake of ^{89}ZrDFO-G3-DARPin was found to be dose-dependent. The flexibility of the DARPin technology for rapid identification of new protein binders, combined with site-specific enzyme-mediated functionalization, is an attractive platform for developing diagnostic and radiotherapeutic radiotracers. Finally, the rapid tumor-targeting and clearance profile of ^{89}ZrDFO-G3-DARPin suggest that DARPin-based radiotracers are potentially suitable for same-day administration and imaging in the clinic.

■ ASSOCIATED CONTENT

Supporting Information

The Supporting Information is available free of charge at https://pubs.acs.org/doi/10.1021/acs.molpharmaceut.2c00136.

Experimental details, NMR spectra, and high-resolution mass spectrometry data for all new compounds, radiochemical data, and additional information on protein expression and purification (PDF)

■ AUTHOR INFORMATION

Corresponding Author

Jason P. Holland − *Department of Chemistry, University of Zurich, 8057 Zurich, Switzerland;* orcid.org/0000-0002-0066-219X; Phone: +41.44.63.53.990; Email: jason.holland@chem.uzh.ch; www.hollandlab.org

Authors

Rachael Fay − *Department of Chemistry, University of Zurich, 8057 Zurich, Switzerland*

Imre Törő − *Department of Biochemistry, University of Zurich, 8057 Zurich, Switzerland*

Anna-Lena Schinke − *Department of Biochemistry, University of Zurich, 8057 Zurich, Switzerland*

Branko Simic − *Department of Biochemistry, University of Zurich, 8057 Zurich, Switzerland*

Jonas V. Schaefer − *Department of Biochemistry, University of Zurich, 8057 Zurich, Switzerland*

Birgit Dreier − *Department of Biochemistry, University of Zurich, 8057 Zurich, Switzerland*

Andreas Plückthun − *Department of Biochemistry, University of Zurich, 8057 Zurich, Switzerland;* orcid.org/0000-0003-4191-5306

Complete contact information is available at: https://pubs.acs.org/10.1021/acs.molpharmaceut.2c00136

Notes

The authors declare no competing financial interest.

■ ACKNOWLEDGMENTS

J.P.H. thanks the Swiss National Science Foundation (SNSF Professorships PP00P2_163683 and PP00P2_190093), the Swiss Cancer Research Foundation (Grant KFS-4257-08-2017), and the University of Zurich (UZH) for financial support. This project has received funding from the European Union's Horizon 2020 research and innovation program from the European Research Council under the Grant Agreement 676904, ERC-StG-2015, NanoSCAN.

■ REFERENCES

(1) Wu, A. M.; Olafsen, T. Antibodies for Molecular Imaging of Cancer. *Cancer J.* **2008**, *14* (3), 191−197.

(2) Wei, W.; Rosenkrans, Z. T.; Liu, J.; Huang, G.; Luo, Q. Y.; Cai, W. ImmunoPET: Concept, Design, and Applications. *Chem. Rev.* **2020**, *120* (8), 3787−3851.

(3) Freise, A. C.; Wu, A. M. In Vivo Imaging with Antibodies and Engineered Fragments. *Mol. Immunol.* **2015**, *67* (2), 142−152.

(4) Olafsen, T.; Wu, A. M. Antibody Vectors for Imaging. *Semin. Nucl. Med.* **2010**, *40* (3), 167−181.

(5) Pandit-Taskar, N.; O'Donoghue, J. A.; Ruan, S.; Lyashchenko, S. K.; Carrasquillo, J. A.; Heller, G.; Martinez, D. F.; Cheal, S. M.; Lewis, J. S.; Fleisher, M.; Keppler, J. S.; Reiter, R. E.; Wu, A. M.; Weber, W. A.; Scher, H. I.; Larson, S. M.; Morris, M. J. First-in-Human Imaging with 89Zr-Df-IAB2M Anti-PSMA Minibody in Patients with Metastatic Prostate Cancer: Pharmacokinetics, Biodistribution, Dosimetry, and Lesion Uptake. *J. Nucl. Med.* **2016**, *57* (12), 1858−1864.

(6) Morris, M. J.; Pandit-Taskar, N.; Carrasquillo, J. A.; O'Donoghue, J. A.; Humm, J.; Lyashchenko, S. K.; Haupt, E. C.; Bander, N. H.; Tagawa, S. T.; Holland, J. P.; Smith-Jones, P. M.; Lewis, J. S.; Solomon, S. B.; Scher, H. I.; Larson, S. M. Phase I Trial of Zirconium 89 (Zr89) Radiolabeled J591 in Metastatic Castration-Resistant Prostate Cancer (MCRPC). *J. Clin. Oncol.* **2013**, *31* (6), 31.

(7) Pandit-Taskar, N.; O'Donoghue, J. A. A.; Beylergil, V.; Lyashchenko, S.; Ruan, S.; Solomon, S. B. B.; Durack, J. C. C.; Carrasquillo, J. A. A.; Lefkowitz, R. A. A.; Gonen, M.; Lewis, J. S. S.; Holland, J. P. P.; Cheal, S. M. M.; Reuter, V. E. E.; Osborne, J. R. R.; Loda, M. F. F.; Smith-Jones, P. M. M.; Weber, W. A. A.; Bander, N. H. H.; Scher, H. I. I.; Morris, M. J. J.; Larson, S. M. M. ^{89}Zr-HuJ591 Immuno-PET Imaging in Patients with Advanced Metastatic Prostate Cancer. *Eur. J. Nucl. Med. Mol. Imaging* **2014**, *41*, 2093−2105.

(8) O'Donoghue, J. A.; Lewis, J. S.; Pandit-Taskar, N.; Fleming, S. E.; Schoder, H.; Larson, S. M.; Beylergil, V.; Ruan, S.; Lyashchenko, S.; Zanzonico, P. B.; Weber, W. A.; Carrasquillo, J. A.; Janjigian, Y. Y. Pharmacokinetics, Biodistribution, and Radiation Dosimetry for ^{89} Zr-Trastuzumab in Patients with Esophagogastric Cancer. *J. Nucl. Med.* **2018**, *59*, 161.

(9) Bensch, F.; Smeenk, M. M.; van Es, S. C.; de Jong, J. R.; Schröder, C. P.; Oosting, S. F.; Lub-de Hooge, M. N.; Menke-van der Houven van Oordt, C. W.; Brouwers, A. H.; Boellaard, R.; de Vries, E. G. E. Comparative Biodistribution Analysis across Four Different ^{89}Zr-Monoclonal Antibody Tracers-The First Step towards an Imaging Warehouse. *Theranostics* **2018**, *8* (16), 4295−4304.

(10) Oosting, S. F.; Brouwers, A. H.; van Es, S. C.; Nagengast, W. B.; Oude Munnink, T. H.; Lub-de Hooge, M. N.; Hollema, H.; de Jong, J. R.; de Jong, I. J.; de Haas, S.; Scherer, S. J.; Sluiter, W. J.; Dierckx, R. A.; Bongaerts, A. H. H.; Gietema, J. A.; de Vries, E. G. E. ^{89}Zr-Bevacizumab PET Visualizes Heterogeneous Tracer Accumulation in Tumor Lesions of Renal Cell Carcinoma Patients and Differential Effects of Antiangiogenic Treatment. *J. Nucl. Med.* **2015**, *56* (1), 63−69.

(11) Wu, A. M.; Senter, P. D. Arming Antibodies: Prospects and Challenges for Immunoconjugates. *Nat. Biotechnol.* **2005**, *23* (9), 1137−1146.
(12) Wu, A. M. Engineered Antibodies for Molecular Imaging of Cancer. *Methods* **2014**, *65* (1), 139−147.
(13) Plückthun, A. Designed Ankyrin Repeat Proteins (DARPins): Binding Proteins for Research, Diagnostics, and Therapy. *Annu. Rev. Pharmacol. Toxicol.* **2015**, *55* (1), 489−511.
(14) Goldstein, R.; Sosabowski, J.; Livanos, M.; Leyton, J.; Vigor, K.; Bhavsar, G.; Nagy-Davidescu, G.; Rashid, M.; Miranda, E.; Yeung, J.; Tolner, B.; Plückthun, A.; Mather, S.; Meyer, T.; Chester, K. Development of the Designed Ankyrin Repeat Protein (DARPin) G3 for HER2 Molecular Imaging. *Eur. J. Nucl. Med. Mol. Imaging* **2015**, *42* (2), 288−301.
(15) Vorobyeva, A.; Bragina, O.; Altai, M.; Mitran, B.; Orlova, A.; Shulga, A.; Proshkina, G.; Chernov, V.; Tolmachev, V.; Deyev, S. Comparative Evaluation of Radioiodine and Technetium-Labeled DARPin 9−29 for Radionuclide Molecular Imaging of HER2 Expression in Malignant Tumors. *Contrast Media Mol. Imaging* **2018**, *2018*, 1−11.
(16) Binz, H. K.; Stumpp, M. T.; Forrer, P.; Amstutz, P.; Plückthun, A. Designing Repeat Proteins: Well-Expressed, Soluble and Stable Proteins from Combinatorial Libraries of Consensus Ankyrin Repeat Proteins. *J. Mol. Biol.* **2003**, *332* (2), 489−503.
(17) Binz, H. K.; Amstutz, P.; Kohl, A.; Stumpp, M. T.; Briand, C.; Forrer, P.; Grütter, M. G.; Plückthun, A. High-Affinity Binders Selected from Designed Ankyrin Repeat Protein Libraries. *Nat. Biotechnol.* **2004**, *22* (5), 575−582.
(18) Kramer, M. A.; Wetzel, S. K.; Plückthun, A.; Mittl, P. R. E.; Grütter, M. G. Structural Determinants for Improved Stability of Designed Ankyrin Repeat Proteins with a Redesigned C-Capping Module. *J. Mol. Biol.* **2010**, *404* (3), 381−391.
(19) Merz, T.; Wetzel, S. K.; Firbank, S.; Plückthun, A.; Grütter, M. G.; Mittl, P. R. E. Stabilizing Ionic Interactions in a Full-Consensus Ankyrin Repeat Protein. *J. Mol. Biol.* **2008**, *376* (1), 232−240.
(20) Zahnd, C.; Kawe, M.; Stumpp, M. T.; De Pasquale, C.; Tamaskovic, R.; Nagy-Davidescu, G.; Dreier, B.; Schibli, R.; Binz, H. K.; Waibel, R.; Plückthun, A. Efficient Tumor Targeting with High-Affinity Designed Ankyrin Repeat Proteins: Effects of Affinity and Molecular Size. *Cancer Res.* **2010**, *70* (4), 1595−1605.
(21) Jost, C.; Schilling, J.; Tamaskovic, R.; Schwill, M.; Honegger, A.; Plückthun, A. Structural Basis for Eliciting a Cytotoxic Effect in HER2-Overexpressing Cancer Cells via Binding to the Extracellular Domain of HER2. *Structure* **2013**, *21* (11), 1979−1991.
(22) Baselga, J.; Coleman, R. E.; Cortés, J.; Janni, W. Advances in the Management of HER2-Positive Early Breast Cancer. *Crit. Rev. Oncol. Hematol.* **2017**, *119*, 113−122.
(23) Baselga, J. Mechanism of Action of Trastuzumab and Scientific Update. *Semin. Oncol.* **2001**, *28*, 4−11.
(24) Waibel, R.; Alberto, R.; Willuda, J.; Finnern, R.; Schibli, R.; Stichelberger, A.; Egli, A.; Abram, U.; Mach, J. P.; Plückthun, A.; Schubiger, P. A. Stable One-Step Technetium-99m Labeling of His-Tagged Recombinant Proteins with a Novel Tc(I)-Carbonyl Complex. *Nat. Biotechnol.* **1999**, *17* (9), 897−901.
(25) Goldstein, R.; Sosabowski, J.; Livanos, M.; Leyton, J.; Vigor, K.; Bhavsar, G.; Nagy-Davidescu, G.; Rashid, M.; Miranda, E.; Yeung, J.; Tolner, B.; Plückthun, A.; Mather, S.; Meyer, T.; Chester, K. Development of the Designed Ankyrin Repeat Protein (DARPin) G3 for HER2 Molecular Imaging. *Eur. J. Nucl. Med. Mol. Imaging* **2015**, *42* (2), 288−301.
(26) Vorobyeva, A.; Schulga, A.; Konovalova, E.; Güler, R.; Mitran, B.; Garousi, J.; Rinne, S.; Löfblom, J.; Orlova, A.; Deyev, S.; Tolmachev, V. Comparison of Tumor-Targeting Properties of Directly and Indirectly Radioiodinated Designed Ankyrin Repeat Protein (DARPin) G3 Variants for Molecular Imaging of HER2. *Int. J. Oncol.* **2019**, *54* (4), 1209−1220.
(27) Deyev, S. M.; Xu, T.; Liu, Y.; Schulga, A.; Konovalova, E.; Garousi, J.; Rinne, S. S.; Larkina, M.; Ding, H.; Gräslund, T.; Orlova, A.; Tolmachev, V.; Vorobyeva, A. Influence of the Position and Composition of Radiometals and Radioiodine Labels on Imaging of Epcam Expression in Prostate Cancer Model Using the Darpin Ec1. *Cancers (Basel)* **2021**, *13* (14), 3589.
(28) Bragina, O.; Chernov, V.; Schulga, A.; Konovalova, E.; Garbukov, E.; Vorobyeva, A.; Orlova, A.; Tashireva, L.; Sorensen, J.; Zelchan, R.; Medvedeva, A.; Deyev, S.; Tolmachev, V. Phase I Trial of ^{99m}Tc-(HE)3-G3, a DARPin-Based Probe for Imaging of HER2 Expression in Breast Cancer. *J. Nucl. Med.* **2022**, *63*, 528.
(29) Pishesha, N.; Ingram, J. R.; Ploegh, H. L. Sortase A: A Model for Transpeptidation and Its Biological Applications. *Ann. Rev. Cell Dev. Biol.* **2018**, *34*, 163−188.
(30) Theile, C. S.; Witte, M. D.; Blom, A. E. M.; Kundrat, L.; Ploegh, H. L.; Guimaraes, C. P. Site-Specific N-Terminal Labeling of Proteins Using Sortase-Mediated Reactions. *Nat. Protoc.* **2013**, *8* (9), 1800−1807.
(31) Guimaraes, C. P.; Witte, M. D.; Theile, C. S.; Bozkurt, G.; Kundrat, L.; Blom, A. E. M.; Ploegh, H. L. Site-Specific C-Terminal and Internal Loop Labeling of Proteins Using Sortase-Mediated Reactions. *Nat. Protoc.* **2013**, *8* (9), 1787−1799.
(32) Naik, M. T.; Suree, N.; Ilangovan, U.; Liew, C. K.; Thieu, W.; Campbell, D. O.; Clemens, J. J.; Jung, M. E.; Clubb, R. T. Staphylococcus Aureus Sortase a Transpeptidase: Calcium Promotes Sorting Signal Binding by Altering the Mobility and Structure of an Active Site Loop. *J. Biol. Chem.* **2006**, *281* (3), 1817−1826.
(33) Hagemeyer, C. E.; Alt, K.; Johnston, A. P. R.; Such, G. K.; Ta, H. T.; Leung, M. K. M.; Prabhu, S.; Wang, X.; Caruso, F.; Peter, K. Particle Generation, Functionalization and Sortase A-Mediated Modification with Targeting of Single-Chain Antibodies for Diagnostic and Therapeutic Use. *Nat. Protoc.* **2015**, *10* (1), 90−105.
(34) Massa, S.; Vikani, N.; Betti, C.; Ballet, S.; Vanderhaegen, S.; Steyaert, J.; Descamps, B.; Vanhove, C.; Bunschoten, A.; van Leeuwen, F. W. B.; Hernot, S.; Caveliers, V.; Lahoutte, T.; Muyldermans, S.; Xavier, C.; Devoogdt, N. Sortase A-Mediated Site-Specific Labeling of Camelid Single-Domain Antibody-Fragments: A Versatile Strategy for Multiple Molecular Imaging Modalities. *Contrast Media Mol. Imaging* **2016**, *11* (5), 328−339.
(35) Paterson, B. M.; Alt, K.; Jeffery, C. M.; Price, R. I.; Jagdale, S.; Rigby, S.; Williams, C. C.; Peter, K.; Hagemeyer, C. E.; Donnelly, P. S. Enzyme-Mediated Site-Specific Bioconjugation of Metal Complexes to Proteins: Sortase-Mediated Coupling of Copper-64 to a Single-Chain Antibody. *Angew. Chemie - Int. Ed.* **2014**, *53* (24), 6115−6119.
(36) Hansen, S.; Stüber, J. C.; Ernst, P.; Koch, A.; Bojar, D.; Batyuk, A.; Plückthun, A. Design and Applications of a Clamp for Green Fluorescent Protein with Picomolar Affinity. *Sci. Rep.* **2017**, *7* (1), 1−16.
(37) Lindmo, T.; Boven, E.; Cuttitta, F.; Fedorko, J.; Bunn, P. A. Determination of the Immunoreactive Function of Radiolabeled Monoclonal Antibodies by Linear Extrapolation to Binding at Infinite Antigen Excess. *J. Immunol. Methods* **1984**, *72* (1), 77−89.
(38) Rashidian, M.; Ingram, J. R.; Dougan, M.; Dongre, A.; Whang, K. A.; LeGall, C.; Cragnolini, J. J.; Bierie, B.; Gostissa, M.; Gorman, J.; Grotenbreg, G. M.; Bhan, A.; Weinberg, R. A.; Ploegh, H. L. Predicting the Response to CTLA-4 Blockade by Longitudinal Noninvasive Monitoring of CD8 T Cells. *J. Exp. Med.* **2017**, *214* (8), 2243−2255.
(39) Rudd, S. E.; Van Zuylekom, J. K.; Raicevic, A.; Pearce, L. A.; Cullinane, C.; Williams, C. C.; Adams, T. E.; Hicks, R. J.; Donnelly, P. S. Enzyme Mediated Incorporation of Zirconium-89 or Copper-64 into a Fragment Antibody for Same Day Imaging of Epidermal Growth Factor Receptor. *Chem. Sci.* **2021**, *12* (26), 9004−9016.
(40) Li, J.; Zhang, Y.; Soubias, O.; Khago, D.; Chao, F. A.; Li, Y.; Shaw, K.; Byrd, R. A. Optimization of Sortase A Ligation for Flexible Engineering of Complex Protein Systems. *J. Biol. Chem.* **2020**, *295* (9), 2664−2675.
(41) Zou, Z.; Mate, D. M.; Nöth, M.; Jakob, F.; Schwaneberg, U. Enhancing Robustness of Sortase A by Loop Engineering and Backbone Cyclization. *Chem. - A Eur. J.* **2020**, *26*, 13568−13572.
(42) Bhatt, N. B.; Pandya, D. N.; Wadas, T. J. Recent Advances in Zirconium-89 Chelator Development. *Molecules* **2018**, *23*, 638.

(43) Stern, L. A.; Case, B. A.; Hackel, B. J. Alternative Non-Antibody Protein Scaffolds for Molecular Imaging of Cancer. *Curr. Opin. Chem. Eng.* **2013**, *2*, 425−432.

(44) Vorobyeva, A.; Schulga, A.; Konovalova, E.; Güler, R.; Löfblom, J.; Sandström, M.; Garousi, J.; Chernov, V.; Bragina, O.; Orlova, A.; Tolmachev, V.; Deyev, S. M. Optimal Composition and Position of Histidine-Containing Tags Improves Biodistribution of ^{99m}Tc-Labeled DARPin G3. *Sci. Rep.* **2019**, *9* (1), 1−11.

(45) Altai, M.; Garousi, J.; Rinne, S. S.; Schulga, A.; Deyev, S.; Vorobyeva, A. On the Prevention of Kidney Uptake of Radiolabeled DARPins. *EJNMMI Res.* **2020**, *10*, 7.

(46) Holland, J. P.; Caldas-Lopes, E.; Divilov, V.; Longo, V. a; Taldone, T.; Zatorska, D.; Chiosis, G.; Lewis, J. S. Measuring the Pharmacodynamic Effects of a Novel Hsp90 Inhibitor on HER2/Neu Expression in Mice Using ^{89}Zr-DFO-Trastuzumab. *PLoS One* **2010**, *5* (1), e8859.

(47) Bensch, F.; Brouwers, A. H.; Lub-de Hooge, M. N.; de Jong, J. R.; van der Vegt, B.; Sleijfer, S.; de Vries, E. G. E.; Schröder, C. P. ^{89}Zr-Trastuzumab PET Supports Clinical Decision Making in Breast Cancer Patients, When HER2 Status Cannot Be Determined by Standard Work Up. *Eur. J. Nucl. Med. Mol. Imaging* **2018**, *45* (13), 2300−2306.

(48) Nord, K.; Gunneriusson, E.; Ringdahl, J.; Stahl, S.; Uhlen, M.; Nygren, P. Binding Proteins Selected from Combinatorial Libraries of an α-Helical Bacterial Receptor Domain. *Nat. Biotechnol.* **1997**, *15*, 772−777.

(49) Dreier, B.; Plückthun, A. Rapid Selection of High-Affinity Binders Using Ribosome Display. *Methods Mol. Biol.* **2012**, *805*, 261−286.

https://doi.org/10.1021/acs.molpharmaceut.2c00136
Mol. Pharmaceutics 2022, 19, 3576−3585